Journal of Structural Geology, Vol. 15, No. 9/10, pp. 1077 to 1095, 1993
Printed in Great Britain

0191-8141/93 $06.00 + 0.00

Dislocation interactions in experimentally deformed biotite

ROY CHRISTOFFERSEN*

Department of Geology, Indiana University, Bloomington, IN 47405, U.S.A.

and

ANDREAS K. KRONENBERG

Center for Tectonophysics, Texas A&M University, College Station, TX 77843, U.S.A.

(*Received* 31 *July* 1992; *accepted in revised form* 9 *February* 1993)

Abstract—Biotite single crystals shortened experimentally in orientations that maximize critical resolved shear stresses on (001) in directions ⟨110⟩, ⟨010⟩ and ⟨310⟩ have been examined by transmission electron microscopy. In all samples, dislocations are confined to the basal plane with Burgers vectors of 1/2⟨110⟩ and ⟨100⟩, consistent with previous determinations of mica slip systems. Occasional partial dislocations that bound stacking faults form extended dislocations of these same systems. Typically dislocations are concentrated in complex arrays in local regions of the samples; isolated or widely spaced dislocations are the exception. Within these arrays, a variety of interactions between the dislocations are suggested by the geometrical arrangements of dislocations that cross over one another on parallel (001) planes sufficiently close together for elastic interaction, and dislocations on the same (001) plane in networks and parallel arrays. Crossing dislocations of opposite sign on separate (001) planes form stable dipole segments where they overlap. Attractive and repulsive interactions between overlapping dislocations of like sign are evident as well. Dislocation networks occur in all samples and may exhibit a variety of complexly distorted geometries. The spacing of dislocations in parallel arrays do not match models for standard dislocation pile-ups, consistent with observations showing these arrays involve dislocation multipoles. The observed dislocation arrays and interactions resemble those reported for Stage I easy-glide deformation of FCC and HCP metals. Basal shear strengths are probably largely controlled by the development of multipoles and dislocations that pile up behind them.

INTRODUCTION

MICAS are weak in shear and at relatively low mean stresses deform by dislocation glide on their basal plane. Undulatory extinction and kink bands due to basal slip are characteristic of the optical microstructures of naturally deformed micas (Bell & Wilson 1977, Wilson & Bell 1979, Wilson 1980, Behrmann 1984, Lister & Snoke 1984, Bell *et al.* 1986, Kanaori *et al.* 1991). Dislocations and associated stacking faults restricted to the (001) basal glide plane are common (Bell & Wilson 1981, Bell *et al.* 1986), and glissile dislocations on non-basal systems have not been observed (Amelinckx 1979). Basal shear strengths measured experimentally for biotite (Kronenberg *et al.* 1990) and muscovite (Mares & Kronenberg 1993) are small relative to the strengths of most other silicates determined at the same conditions (e.g. Kirby 1985, Carter & Tsenn 1987, Evans & Dresen 1991). Easy (001) slip is responsible for deformation of micas compressed in nearly all orientations, including those that give rise to kinking (Borg & Handin 1966, Etheridge *et al.* 1973, Bell *et al.* 1986, Mares & Kronenberg 1993).

The role of (001) slip in the development of kink bands in micas has been investigated by transmission electron microscopy (TEM) (Bell *et al.* 1986) of experimentally deformed biotite crystals loaded parallel to cleavage (Etheridge *et al.* 1973). Contrary to previous, simple models for kink bands and crystallographic constraints across their boundaries (Frank & Stroh 1952, Starkey 1968, Baronnet & Olives 1983), Bell *et al.* (1986) showed that the boundaries of sharply defined, optical-scale kink bands consist of complex staggered and dilatant boundaries with multiple cleavage cracks spaced along them. Early in the development of high-angle kink band boundaries, however, dislocations organize into low-angle tilt (and twist) walls and serve as nucleii for dilatant, high-angle boundaries. No evidence for dislocation climb was reported for these samples (Bell *et al.* 1986), and dislocations appear to organize by glide in response to elastic interactions between dislocations in nearby parallel glide planes.

Kronenberg *et al.* (1990) reported optical evidence for dislocation organization and mechanical evidence for dislocation interaction in biotite crystals loaded at 45° to (001), favoring basal slip. In these samples, true kink bands with sharply defined, high-angle boundaries (that have opposite senses of rotation) occurred only at sample corners. However, low-angle (0.5–5°) tilt walls or kink boundaries (KBs) were apparent normal to the basal plane, spaced throughout samples. Neighboring kink boundaries within sample interiors may have the same or opposite senses of rotation and thus do not always define kink bands.

In this paper, we report the results of TEM investi-

*Current address: Department of Materials Science, University of Pennsylvania, 3231 Walnut Street, Philadelphia, PA 19104, U.S.A.

gations of these samples with the goal of identifying the dislocation interactions that are involved in the early stages of kink band development and that limit dislocation mobility. We observe evidence for dislocation interactions that includes finite dipole segments formed by attractive forces between crossing dislocations on separate (001) planes, repulsion between parallel dislocations that form large arrays on the same (001) glide plane, and networks formed by the reaction of dislocations gliding on the same plane. As a result of these interactions, complex dislocation arrays develop, including multiple dipoles (multipoles) that may be expected to limit dislocation mobility. Shear strengths and low-angle KB spacings in these samples show a crude correlation. However, neither the length scales defined by KBs nor the observed dislocation spacings are consistent with simple pile-up models. The dislocation substructures we observe are compared with those of metals in which slip is restricted to a single plane. We borrow deformation models developed for metal and other systems that use dislocation trapping and accumulation to explain observed glide strengths.

EXPERIMENTAL PROCEDURES

The biotite samples examined in this study were deformed experimentally by shortening single crystals at 45° to (001), using an internally heated Heard-type gas apparatus (Kronenberg *et al.* 1990). The average chemical composition of the samples was $K_{1.69}Na_{0.171}(Fe^{2+}_{1.82}Mg_{3.50}Mn_{0.068})(Fe^{3+}_{0.117}Ti_{0.230})(Si_{5.92}Al_{2.15}O_{20})(OH_{1.58}F_{2.42})$, and was determined from electron microprobe analyses and independent Fe^{3+}/Fe^{2+} determinations.

The dislocation substructures of selected samples (Table 1) were examined by TEM of (001)-parallel foils prepared by gently pulling cleavage flakes from the surface of the samples with a piece of adhesive tape and removing the tape adhesive with acetone (see Silk & Barnes 1961). This was usually sufficient to produce foils with large electron-transparent regions, although a short duration of ion milling was sometimes needed to clean the specimen surface or to increase the amount of thin area. Because the corners and edges of the experimental samples were often highly kinked and inhomogeneously deformed, TEM observations were restricted to foils obtained from the more homogeneously deformed interiors of the samples. Transmission electron microscopy was carried out at 120 kV, with Philips 400T instruments located at Texas A&M University and the University of Pennsylvania. A cryogenic double-tilt sample holder was used in order to eliminate the rapid electron beam damage effects that are characteristic of biotite.

MECHANICAL BEHAVIOR

Measured variations in shear strength with shear direction in the basal plane of biotite (Fig. 1) suggest that (001) dislocations interfere with their mutual advance (Kronenberg *et al.* 1990), particularly in the directions ⟨310⟩ and ⟨010⟩ that require the activation of multiple slip systems. Basal shear strengths ($\tau_{001} = (\sigma_1 - \sigma_3)/2$) determined from triaxial compression experiments performed at constant strain rates on single crystals loaded at 45° to (001) reach nearly constant values soon after the onset of yielding (Fig. 1a), with little or no strain hardening or softening. Shear strengths determined in the ⟨100⟩ and ⟨110⟩ directions are lower than those for shear in the ⟨310⟩ and ⟨010⟩ directions (Fig. 1b), consistent with the slip vectors **b** = ⟨100⟩ and 1/2⟨110⟩ reported for micas (Silk & Barnes 1961, Demny 1963a,b, Etheridge *et al.* 1973, Bell & Wilson 1981, Bell *et al.* 1986, Meike 1989). Shear in ⟨310⟩ or ⟨010⟩ directions requires the simultaneous operation of two systems of dislo-

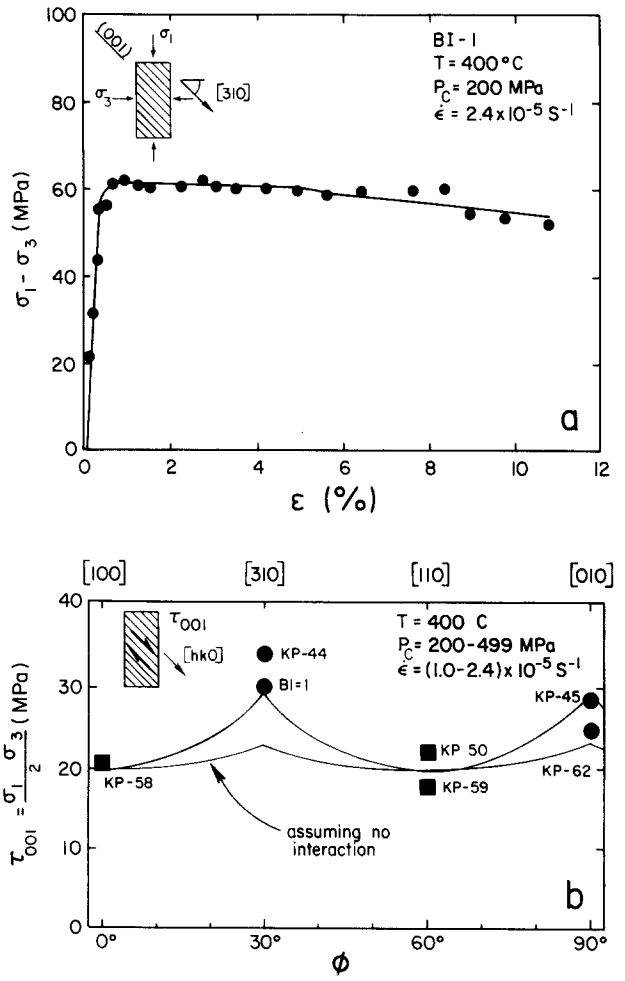

Fig. 1. Mechanical results for biotite single crystals compressed at 45° to (001) at T = 400°C, P_c = 200–499 MPa, and $\dot{\varepsilon}$ = (1.0–2.4) × 10^{-5} s^{-1}. (a) Differential stress ($\sigma_1 - \sigma_3$) vs axial strain ε for sample BI-1 loaded at 45° to ⟨310⟩. The yield point is sharply defined and differential stresses measured at $\varepsilon > 1\%$ are nearly constant. (b) Shear stress τ on (001) required for slip (taking $(\sigma_1 - \sigma_3)/2$ at ε = 5%) as a function of slip direction ϕ within (001) where ϕ is measured from the a-axis. Minimum shear strengths correspond to the dislocation slip vectors **b** = ⟨100⟩ and **b** = 1/2⟨110⟩. Shear strengths measured for intermediate directions [310] and [010] that require multiple slip are larger than predicted by Schmid's law and the strengths measured in [100] and [110] directions assuming no interactions between dislocations. Data for experiments KP-59 and KP-62 correspond to the first steps of strain rate stepping experiments and provide a measure of sample-to-sample variability (after Kronenberg *et al.* 1990).

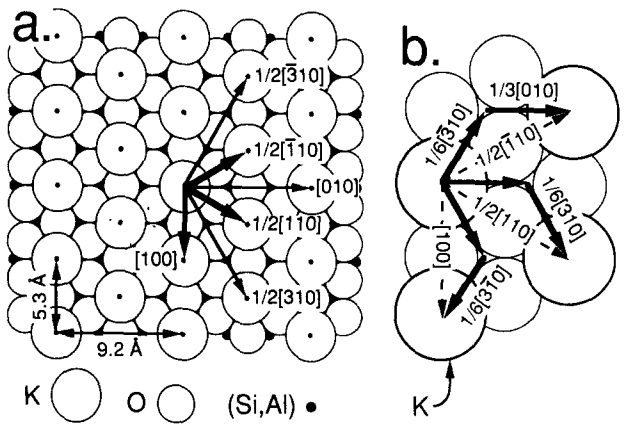

Fig. 2 (a) Structure of K interlayer of biotite (monoclinic, space group C2/m) showing lattice points (small dots) and possible Burgers vectors (arrows) for perfect dislocations. Lattice vectors [100], 1/2[110], 1/2[1̄10] and their symmetrically related equivalents are the principal Burgers vectors for basal slip in biotite. The lattice vectors [010], 1/2[310], 1/2[3̄10] and symmetrical equivalents are longer and have not been reported as Burgers vectors in biotite. Slip in these directions can be produced by combining the shorter ⟨100⟩ and 1/2⟨110⟩ vectors. (b) Structure of K interlayer showing partial Burgers vectors (solid arrows) that may form extended dislocations of the principal slip systems (dotted arrows).

cations that have lower Schmid factors, such as **b** = [100] and 1/2[110] for 1/2[310] slip, and **b** = 1/2[110] and 1/2[1̄10] for [010] slip (Fig. 2a). Shear strengths in these orientations may therefore be expected to be larger than those measured for ⟨100⟩ and ⟨110⟩ samples. However, the strength contrast between shear directions ⟨100⟩ and ⟨110⟩ that are parallel to slip vectors and intermediate directions ⟨310⟩ and ⟨010⟩ that require multiple slip is greater than expected if slip systems operate independently and shear stresses are dictated by critical resolved shear stresses. Assuming no interactions between dislocations, shear strengths in intermediate directions predicted by Schmid's law exceed the critical resolved shear stresses of the principal slip directions by only ~15% (Fig. 1b), below experimental resolution given to sample-to-sample variations for any one orientation.

OPTICAL OBSERVATIONS

The experimentally deformed biotite samples selected for the present study are listed in Table 1 with a summary of the experimental conditions. On the optical scale, low-angle KBs are visible in thin section throughout the interiors of all of our experimentally deformed biotite samples (Fig. 4a). We find that the spacing of these boundaries (Table 1) appears to correlate with the strength variations we observed for samples sheared in different directions in the basal plane. Neglecting sharply defined, high-angle kink bands at sample corners and undeformed regions of samples, low-angle KBs are spaced between 20 and 100 μm. Measured along traverses normal to the KBs, lengths, L, between low-angle KBs have a highly non-Gaussian distribution (Fig. 3) with a peak (L_p) due to numerous, finely spaced KBs in deformed portions of samples. The mean L_m is affected by measured values of L trailing out to ~1–3 mm in relatively undeformed portions of the sample. Nevertheless, using either L_p or L_m as a measure of KB spacing, low-angle KBs are spaced more closely in the stronger samples oriented for shear in the ⟨310⟩ and ⟨010⟩ directions (Fig. 3). The development of low-angle KBs by the accumulation of dislocations of like sign suggests a length scale to dislocation glide, and a relationship between shear stress and the dimensions of dislocation pile-ups approximating $\tau \propto 1/L$ may be anticipated (Eshelby *et al.* 1951). The nature of obstacles to basal glide in biotite single crystals is not known, however, and one of the goals of our TEM study was to determine the mechanisms by which dislocations become localized and low-angle KBs are formed.

TEM OBSERVATIONS

General dislocation substructure

In all samples, including the undeformed starting material, the distribution of dislocations was found to be very inhomogeneous. Foils prepared from the undeformed starting material can contain local regions of high dislocation density, but densities averaged over many TEM plates are on the order of only 2×10^4–4×10^4 mm^{-2}. For the starting materials, generally 2% of a given foil contained dislocations, as compared with 20–30% for foils of the deformed samples. The low density of dislocations in foils of the starting material confirmed that the cleavage method of preparing the TEM samples did not introduce large numbers of dislocations.

Because dislocations in biotite are confined to the (001) basal-plane, and the (001) cleavage foils were uniformly thin over large regions, it was often possible to trace individual dislocation lines and arrays of dislocations over areas of several tens of μm^2. In most cases dislocations tend to be curvilinear, and thus of mixed character (Fig. 4b). The curvilinear line geometry is consistent with the previous observation by Meike (1989), and indicates that Peierls valleys in biotite are shallow.

Within regions containing many dislocations, the local substructure is characterized by various combinations of dislocation networks, arrays of parallel dislocations, and overlapping nets of dislocations on separate (001) planes (Figs. 4c & d). The detailed configurations of these features, and their sample-to-sample variations, are the topics of later sections. In some areas, multiple overlapping arrays of very closely spaced dislocations occur, producing complex strain contrast and Moiré fringes (Fig. 4c). We suspect that in some of these latter areas local separation of the crystal along (001) cleavage planes occurs within the foil.

Slip systems

Burgers vector analysis was carried out using conventional bright-field and dark-field two-beam contrast ex-

Table 1. Experimentally deformed biotite samples*

Sample No.	Shear direction	Shear stress on basal plane, τ_{001} (MPa)	Deformation conditions			Optical kink boundary spacing		TEM
			T (°C)	P_c (MPa)	$\dot{\varepsilon}$ (s^{-1})	Mean, L_m (μm)	Most frequent, L_p (μm)	
KP-77	[100]	23	200	330	1.4×10^{-5}	310 ($^{+540}_{-310}$)	36 ($^{+14}_{-11}$)	No
KP-58	[100]	20.5	400	330	1.1×10^{-5}	450 ($^{+560}_{-450}$)	76 ($^{+84}_{-51}$)	No
BI-1	[310]	30	400	200	2.4×10^{-5}	59 (± 58)	24 ($^{+38}_{-12}$)	No
KP-44	[310]	34	400	330	1.0×10^{-5}	86 ($^{+144}_{-86}$)	36 ($^{+14}_{-11}$)	Yes
KP-67	[110]	38.5	20	330	1.6×10^{-5}	240 ($^{+460}_{-240}$)	64 ($^{+73}_{-51}$)	Yes
KP-65	[110]	27.5	200	330	1.5×10^{-5}	84 ($^{+100}_{-84}$)	29 ($^{+21}_{-17}$)	Yes
KP-50	[110]	21.5	400	300	1.1×10^{-5}	330 ($^{+630}_{-330}$)	66 ($^{+34}_{-28}$)	Yes
BI-3	[010]	60	19	300	2.3×10^{-5}	100 ($^{+280}_{-100}$)	29 ($^{+21}_{-17}$)	Yes
KP-75	[010]	22.5	200	330	1.4×10^{-5}	370 ($^{+510}_{-370}$)	82 ($^{+93}_{-57}$)	Yes
KP-45	[010]	28.5	400	330	1.2×10^{-5}	170 ($^{+330}_{-170}$)	31 ($^{+31}_{-19}$)	Yes

*Samples loaded triaxially with maximum principal stress σ_1 at 45° to (001) (Kronenberg *et al.* 1990).

periments. These methods have the usual limitations with regard to complete invisibility of dislocations in an elastically anisotropic material such as biotite, and without numerical contrast simulation they can only provide information about Burgers vector direction, not magnitude. Dislocations and their Burgers vectors are confined to the basal (001) plane of micas, and evidence for climb has not been reported (Silk & Barnes 1961, Amelinckx & Delavignette 1962, Demny 1963a,b, Bell and Wilson 1981, Bell *et al.* 1986, Meike 1989). Previous work (Baños *et al.* 1983), has also indicated that the likely structural location for (001) slip is on the weakly bonded K interlayer (Fig. 2a). These restrictions, together with the symmetry of the biotite crystal structure, help to facilitate Burgers vectors analysis by placing constraints on likely orientations and magnitudes for the Burgers vectors of perfect dislocations. They also simplify the TEM contrast experiments by requiring invisibility for only one value of **g**. Another advantage for edge dislocations was that the invisibility criteria of both $\mathbf{g}\cdot\mathbf{b} = 0$ and $\mathbf{g}\cdot\mathbf{b}\times\mathbf{u} = 0$ were always obeyed for $hk0$ reflections.

The symmetrically equivalent set 1/2⟨110⟩, and the *a*-axis ⟨100⟩, which is close in magnitude to 1/2⟨110⟩, are the shortest lattice vectors in the basal plane of biotite (Fig. 2a). These principal vectors are the only Burgers vectors reported for perfect dislocations in mica by previous workers (Silk & Barnes 1961, Demny 1963a,b, Bell & Wilson 1981, Bell *et al.* 1986, Meike 1989). The set $\mathbf{b} = 1/2\langle 310\rangle$ and $\mathbf{b} = \langle 010\rangle$ are considerably longer and have not been observed (Fig. 2a). These longer displacement vectors can, however, be obtained by adding two of the shorter Burgers vectors. For example, net slip in the [010] direction may be accomplished by the sequential passage of 1/2[110] and 1/2[$\bar{1}$10] dislocations on the same slip plane. However, repulsive interactions between these particular dislocations may cause them mutually to trap one another and so limit their mobility.

In the present study we found no apparent differences in the dislocation substructure as a function of temperature, and see no evidence that slip systems in particular change with temperature. In samples sheared along ⟨110⟩, dislocations with Burgers vectors 1/2[110] occur together in the same foil with dislocations with the symmetrically equivalent vector 1/2[$\bar{1}$10], and the vector [100]. For shear parallel to ⟨110⟩, two of the potential Burgers vectors are oriented at 60° to the principal shear stress, while the third has a Burgers vector parallel to it (Fig. 2a). Although dislocations with $\mathbf{b} = 1/2[110]$ could produce the needed slip by acting alone, dislocations from the other two systems observed in our samples may have formed at sources where locally heterogeneous stress occur.

In samples sheared along ⟨010⟩ and ⟨310⟩, slip requires activation of two of the principal slip systems with vectors oriented at 30° to the principal shear stress (e.g. 1/2[110] and 1/2[$\bar{1}$10] for shear along [010]), and our contrast experiments confirm the presence of such complementary dislocations in samples sheared in the directions ⟨010⟩ and ⟨310⟩. In networks in these samples, we also find dislocations with Burgers vectors normal to the shear direction (e.g. $\mathbf{b} = [100]$ in networks in samples sheared along [010]), and these are described in the section below on networks.

Partial dislocations

Calculations of stacking fault energies (Baños 1985) for muscovite predict that unit dislocations in mica may dissociate into partial dislocations, with stacking fault widths of 0.7–1.5 nm. Partial dislocations in muscovite and biotite have previously been reported which, combined with appropriate stacking faults, form extended dislocations, with various possible combinations of partial Burgers vectors (Fig. 2b) (Bell & Wilson 1981, Meike 1989). While equilibrium stacking fault widths are narrow, dissociation of dislocations in biotite by as much as 0.5 μm has been observed during *in situ* deformation of foils in a high-voltage TEM, followed by rejoining of the partials after obstacles to glide had been passed (Meike 1989).

Although visibly dissociated dislocations are not commonly observed under static conditions (Silk & Barnes 1961, Amelinckx & Delavignette 1962, Demny 1962a,b), we found some evidence for widely spaced

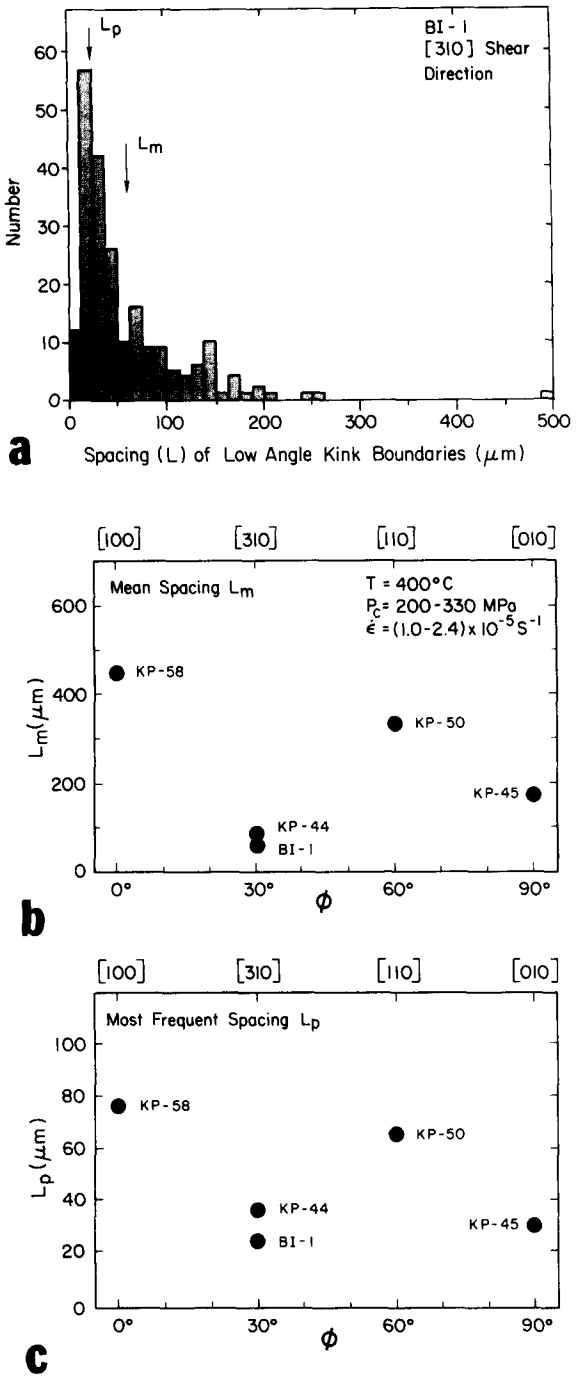

Fig. 3. (a) Histogram of optically measured spacing of low-angle kink boundaries in experimentally deformed sample BI-1. The mean spacing L_m and the peak or most frequent spacing L_p differ significantly due to the strongly asymmetric distribution. (b) & (c) The mean spacing L_m (b) and most frequent spacing L_p (c) of low-angle KBs as a function of slip direction ϕ (see Fig. 1) in biotite single crystals compressed at 45° to (001). Both L_m and L_p show systematic variations with ϕ, with larger values of L for samples sheared in the principal slip directions ⟨100⟩ and ⟨110⟩ than in those sheared in intermediate orientations ⟨310⟩ and ⟨010⟩.

partial dislocations in our samples. Figures 5(a) & (b) show a pair of straight, parallel dislocations that maintain a separation of 0.5–0.8 μm for a distance of up to 20 μm. Nearly perfect invisibility is obtained for one member of the pair for $\mathbf{g} = 130$, consistent with a partial vector $\mathbf{b} = 1/6\langle\bar{3}10\rangle$. We note in this particular case that the stacking fault between the partials shows no strong difference in contrast relative to the unfaulted crystal. Such a lack of contrast is not unusual for stacking faults in layered structures oriented parallel to the plane of the foil, particularly if the fault is close to the surface of the crystal (Amelinckx & Van Landuyt 1976, Amelinckx & Delavignette 1963).

The dissociation width indicated by this pair of dislocations is consistent with Meike's (1989) observations of actively gliding dislocations in biotite. The presence of such widely separated partials under static conditions we believe may be due to internal stresses left within the sample. Overall, we found very few instances of visibly dissociated dislocations, and such features appear to be rare in unstressed biotite.

Parallel dislocation arrays

The majority of the dislocation configurations observed in our deformed biotite samples result from the interaction between dislocations gliding on the same plane or on closely spaced parallel planes. One of the principal configurations produced by dislocations within the same plane are arrays of multiple parallel dislocations with relatively straight or smoothly curving line orientations. In most cases, contrast experiments show that dislocations within these arrays had parallel Burgers vectors. The number of dislocations within these arrays is commonly around 20–30, but larger arrays with as many as 70–100 dislocations also occur. Figure 5(c) shows a portion of one of these larger arrays that contains a total of 60 dislocations.

Although the spacing of the dislocations within parallel arrays appears to be determined by repulsive forces between the dislocations, such as occur in dislocation pile-ups, the spacings as a group do not follow the systematic relationships expected for standard pile-ups (Eshelby *et al.* 1951, Hazzledine & Hirsch 1967). Another difference from standard pile-ups was the apparent lack of inclusions, precipitates or other barriers associated with the arrays. Some obstacles to glide at the head of pile-ups may have been removed during foil preparation. However, high-angle KBs in mica may be effective obstacles to glide due to the large change in crystallographic orientation across their boundaries. Well-defined KBs have been observed in our foils. Moreover, we continue to find unrelaxed dislocation arrangements of other types in foils that reflect residual internal stresses. Study of foils containing several well-developed high-angle KBs revealed that most boundaries are defined by sharp bending points with locally high dislocation densities, but clearly defined pile-ups do not occur adjacent to the boundaries.

In an effort to characterize the parallel dislocation arrays more fully, and compare them with known pile-up models, we measured the dislocation spacings in arrays in two samples, KP-75 and KP-50. In contrast to pile-up models, which predict the dislocation-pair spacing to change systematically with distance (Eshelby *et al.* 1951, Hazzledine & Hirsch 1967), the spacings we measured were quite uniform (0.54 ± 0.25 μm in KP-75 and 0.47 ± 0.17 μm in KP-50), and varied more or less randomly with distance across the arrays. These results,

in addition to the difficulty in locating obstacles at the head of pile-ups, suggest that the nature of the parallel dislocation arrays differs from that of simple pile-ups. Spacings of dislocations on one glide plane may be influenced by dislocations on overlapping, parallel planes, and dislocations in parallel planes may form multiple dipole pairs, also called multipoles (Mader 1963, Steeds & Hazzledine 1964, Hirsch & Lally 1965). Direct evidence for the presence of multipoles in our samples was found in sample KP-50, in which pairs of dislocations within a parallel array merge and become superposed (see below).

Dislocation networks

In addition to forming parallel arrays, dislocations located on the same glide plane can intersect and react to form networks if they have appropriate Burgers vectors. Because climb is difficult, networks form exclusively by the intersection and reaction of dislocations during glide. Networks occur in all samples, but our observations suggest that they are more common in samples sheared in the slip direction ⟨110⟩ vs the non-slip directions ⟨010⟩ and ⟨310⟩. Within individual TEM samples, the extent of well-developed networks and their geometries are highly variable, and it is possible to find isolated nodes at the intersection of just a few dislocations, as well as extended networks measuring several tens of microns across (Fig. 6a). Network geometries include well-developed hexagonal nets (Fig. 6b), orthogonal nets (Fig. 6c), and distorted nets with dislocation segments of very different length and/or curvature (Fig. 7).

As previously discussed, the Burgers vectors for dislocations in biotite are restricted to the shortest lattice vectors 1/2⟨110⟩ and ⟨100⟩. Our contrast experiments are consistent with Burgers vectors based on this set for networks in the ⟨110⟩ shear-direction samples, and also the ⟨010⟩ and ⟨310⟩ samples (Fig. 7). For the ⟨010⟩ and ⟨310⟩ samples, networks contain one set of dislocations whose Burgers vectors are at 90° to the shear direction, such as segments with $\mathbf{b} = \langle 100 \rangle$ in networks in ⟨010⟩ shear-direction samples (Fig. 7). These dislocations have zero resolved shear stress on average, and we did not find them as independent, unreacted dislocations outside of networks. This suggests there are few independent sources for these dislocations, and that the segments we observe form almost exclusively by the reaction of other, mobile dislocations whose Burgers vectors are in more favorable orientations for glide. Our observation that networks appear to be less common in ⟨010⟩ and ⟨310⟩ samples may be related to the fact that the networks in these samples form dislocation segments that are sessile because of their orientations relative to the applied shear stress.

One goal in characterizing networks was to see if the ⟨010⟩ and ⟨310⟩ shear-direction samples might have some networks containing short dislocation segments with ⟨010⟩ or 1/2⟨310⟩ Burgers vectors, respectively. For the example of ⟨010⟩ shear, such a dislocation can form from the combination of principal slip dislocations by reactions like $1/2[110] + 1/2[\bar{1}10] = [010]$. However, we found no evidence for networks containing even short dislocation segments with ⟨010⟩ or 1/2⟨310⟩ vectors. Thus, even though these vectors are in optimal orientations relative to the shear direction, their high energy relative to those of the shorter slip vectors apparently suppresses their formation. Dislocations with Burgers vectors such as $1/2[110]$ and $1/2[\bar{1}10]$ within the same glide plane must therefore interact repulsively, preventing them from passing one another by reaction.

Superposed and crossing dislocations

In addition to features formed by dislocations sharing the same (001) glide plane, all samples contain areas with multiple dislocations located on separate, parallel (001) planes. If they have non-parallel line orientations, these dislocations may cross over one another, or appear to merge into a single dislocation line. Where dislocations cross, they may show little or no change in their line orientations (Fig. 8a), or they may curve to adopt line orientations that are locally more parallel (Fig. 8b), or perpendicular (Fig. 8c). The latter configuration, which is consistent with repulsive interaction between the two dislocations, is considerably less common than the first two. In instances where crossing dislocations adopt locally parallel and superposed orientation due to mutual attraction, the resulting configuration is similar to the pair of nodes in a network. In these cases, contrast experiments were needed to confirm that the overlapping segment of the two dislocations is not a unique dislocation with a different Burger vector. Our observations of locally attractive and repulsive bending of crossing dislocations are similar to those made in a number of other materials (Amelinckx & Delavignette 1962, Mader 1963, Hirsch & Lally 1965, Zhang & Li 1989).

While there are several possible combinations for the Burgers vectors of crossing dislocations, we found those that crossed with attractive-type interactions, or merged into a single line, typically became extinct for the same $\mathbf{g}$, indicating that their Burgers vectors were parallel. Based on this extinction behavior alone, the dislocations can be of the same sign, forming a dipole, or of opposite sign. Where feasible, we applied various criteria to determine whether a segment of superposed dislocations consisted of dislocations of the same or opposite sign. In some cases weak-beam techniques were used to see if it was possible to resolve both members of the dislocation pair (Fig. 8d). If these techniques revealed a finite separation of the dislocations, this was taken as evidence that the pair was a dipole, because dislocation dipoles of edge character are expected to be offset by a projected distance l_x within their slip planes, whereas stable configurations of like-sign dislocations should have no stacking offset (Cottrell 1956). Typically we found that resolvable dislocations in dipoles had projected separations on the order of 30–40 nm (Fig. 8d). Superposed dislocations with no resolvable stacking

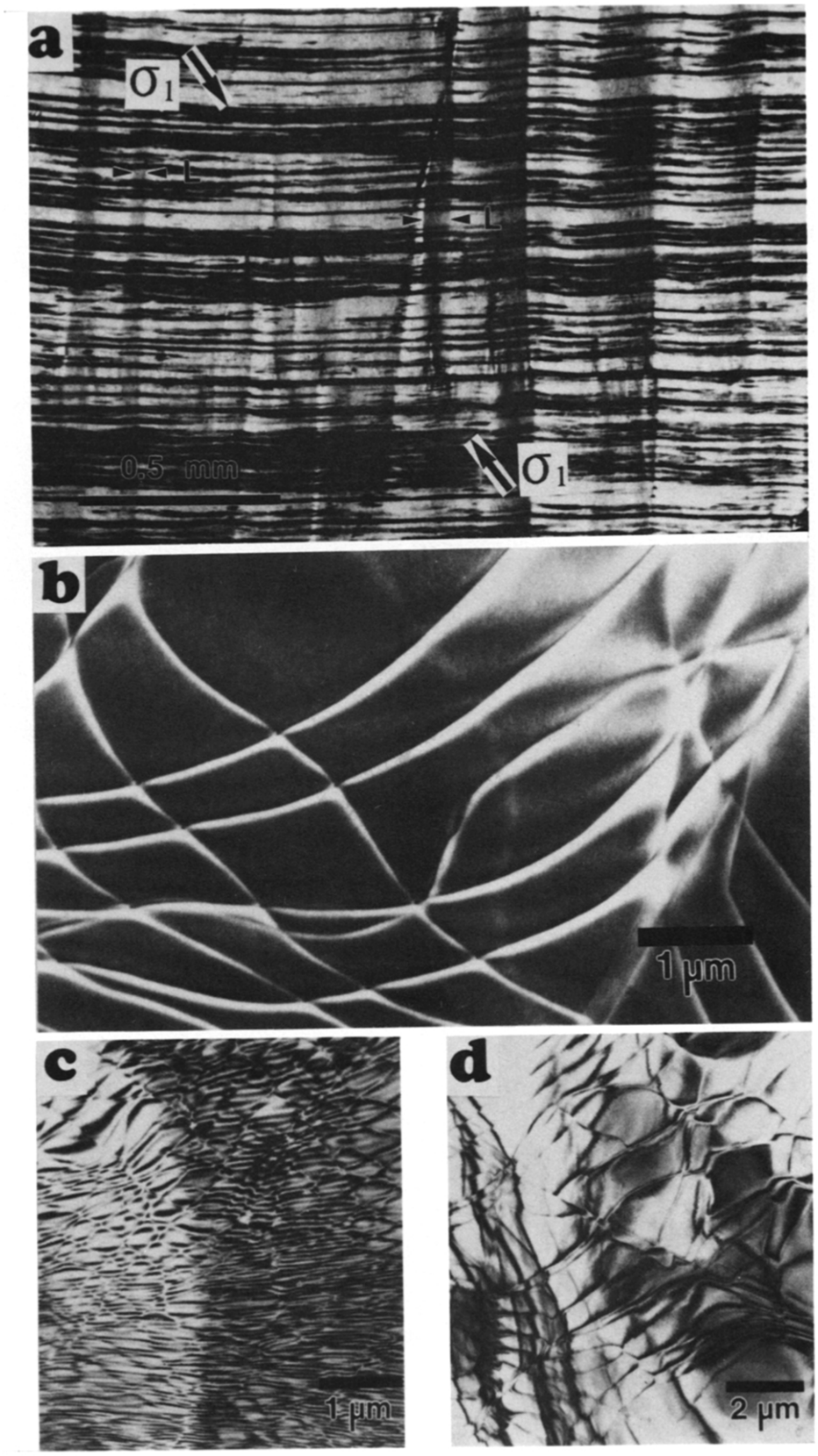

Fig. 4. (a) Optical micrograph of low-angle kink boundaries in experimentally deformed sample BI-1, loaded at 45° to (001) and [310]. The spacings L between low-angle (0.5–5°) kink boundaries were measured in traverses perpendicular to their orientation (crossed nicols). (b) Dark-field image ($\mathbf{g} = 201$) showing dislocations with curvilinear line geometry characteristic of all samples (sample KP-75). (c) Bright-field image of region with high-density of closely-spaced dislocations (sample KP-65). Individual dislocations are locally obscured by Moiré fringes possibly associated with (001) cleavage cracks. (d) Bright-field image of typical concentration of dislocations in experimentally deformed biotite (sample KP-50). Dislocation networks as well as crossing dislocations on parallel (001) planes are visible.

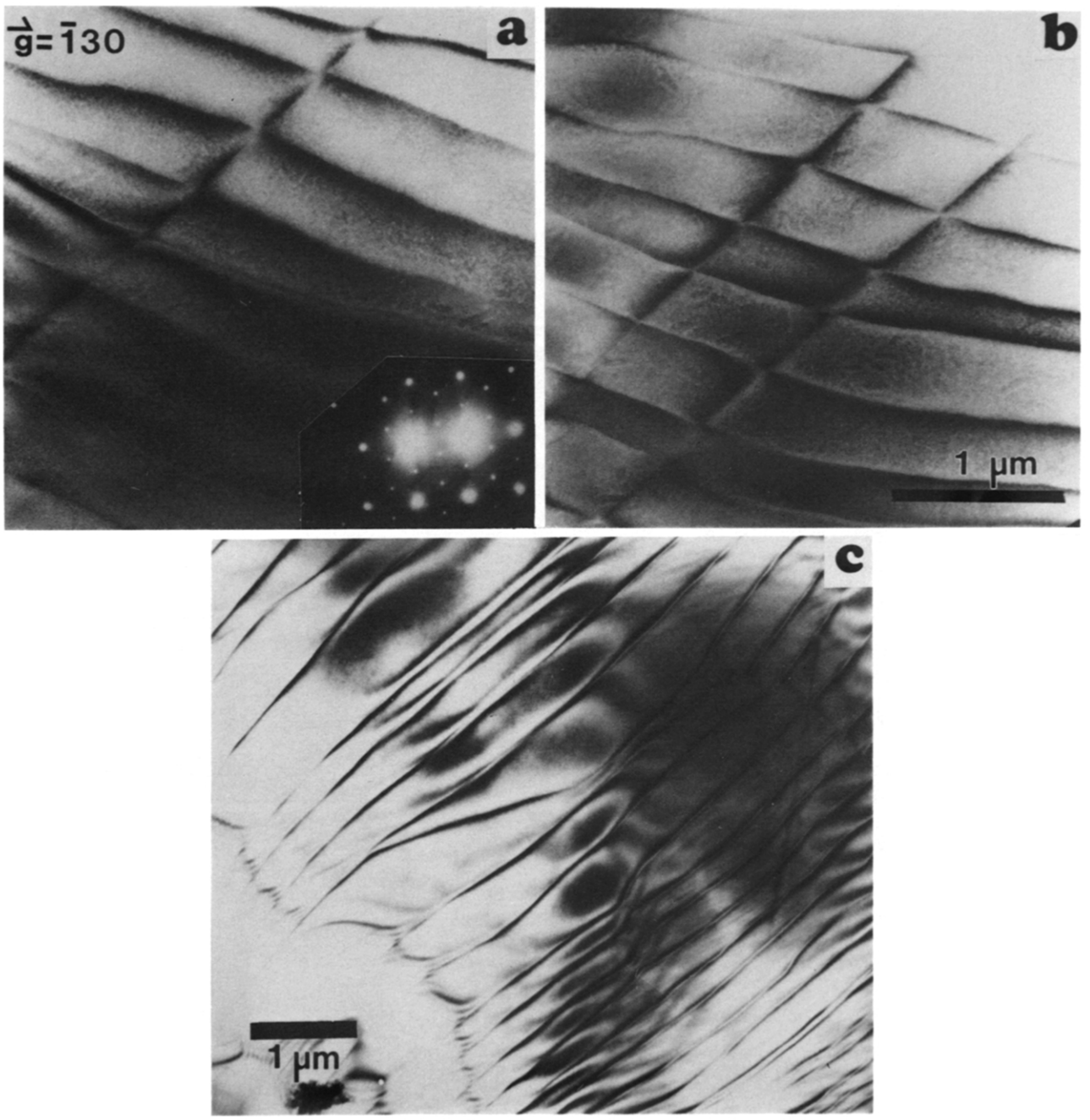

Fig. 5. (a) Pair of parallel dislocations in sample KP-75 under two-beam condition with $\mathbf{g} = 130$ showing nearly complete invisibility for one dislocation; consistent with partial Burgers vector $1/6[\bar{3}10]$. (b) Same dislocation pair under general bright-field diffraction conditions with both dislocations in contrast. (c) Bright-field image of part of an extended array of parallel dislocations within the same glide plane. Apparent doubling of some members of the array is an artifact of the imaging conditions and does not indicate the presence of dipoles or dissociated dislocations.

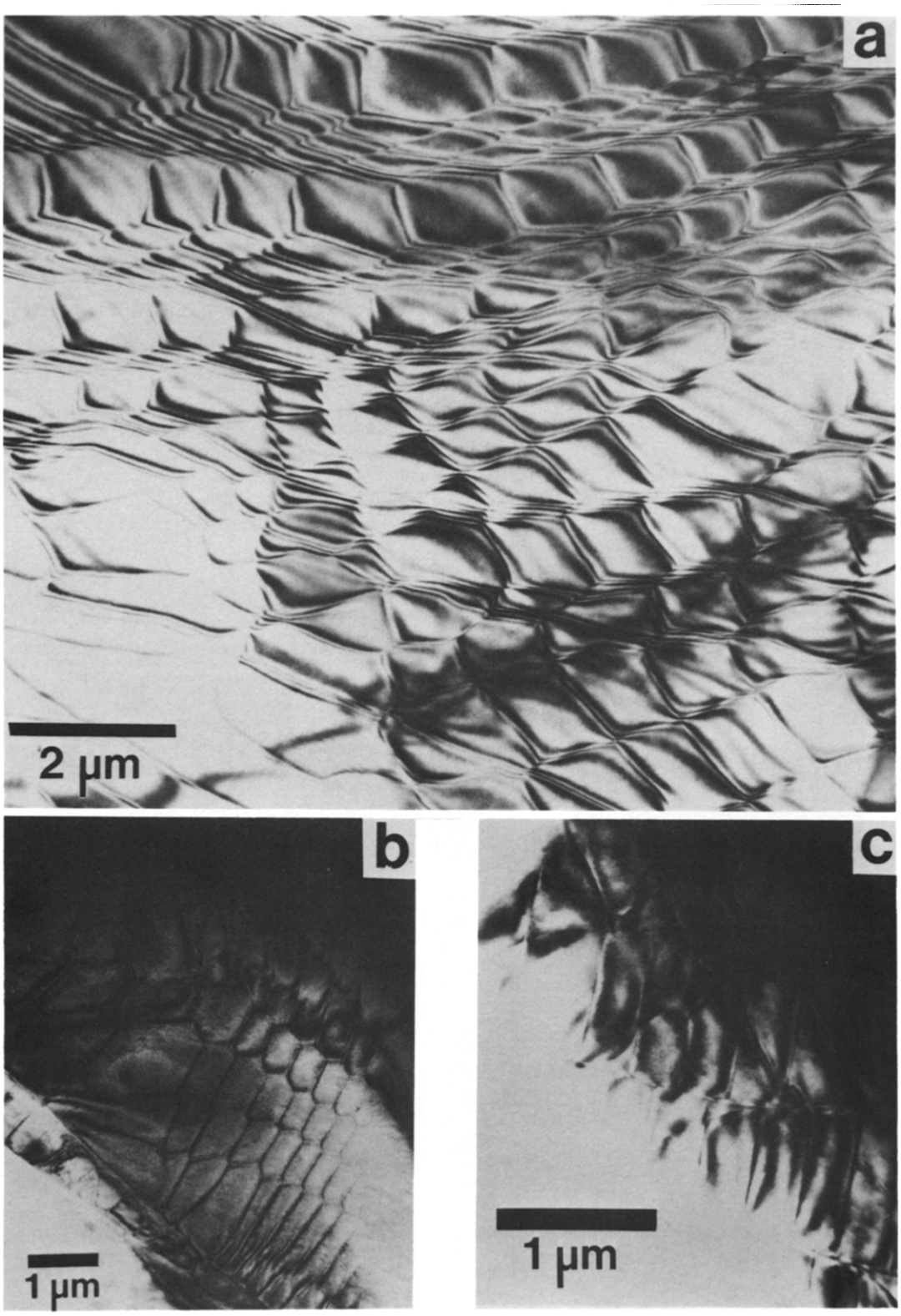

Fig. 6. (a) Bright-field image of portion of extended network with complex geometry in sample KP-50. (b) Hexagonal geometry network (bright-field, sample KP-50). (c) Orthogonal geometry network (bright-field, sample KP-45).

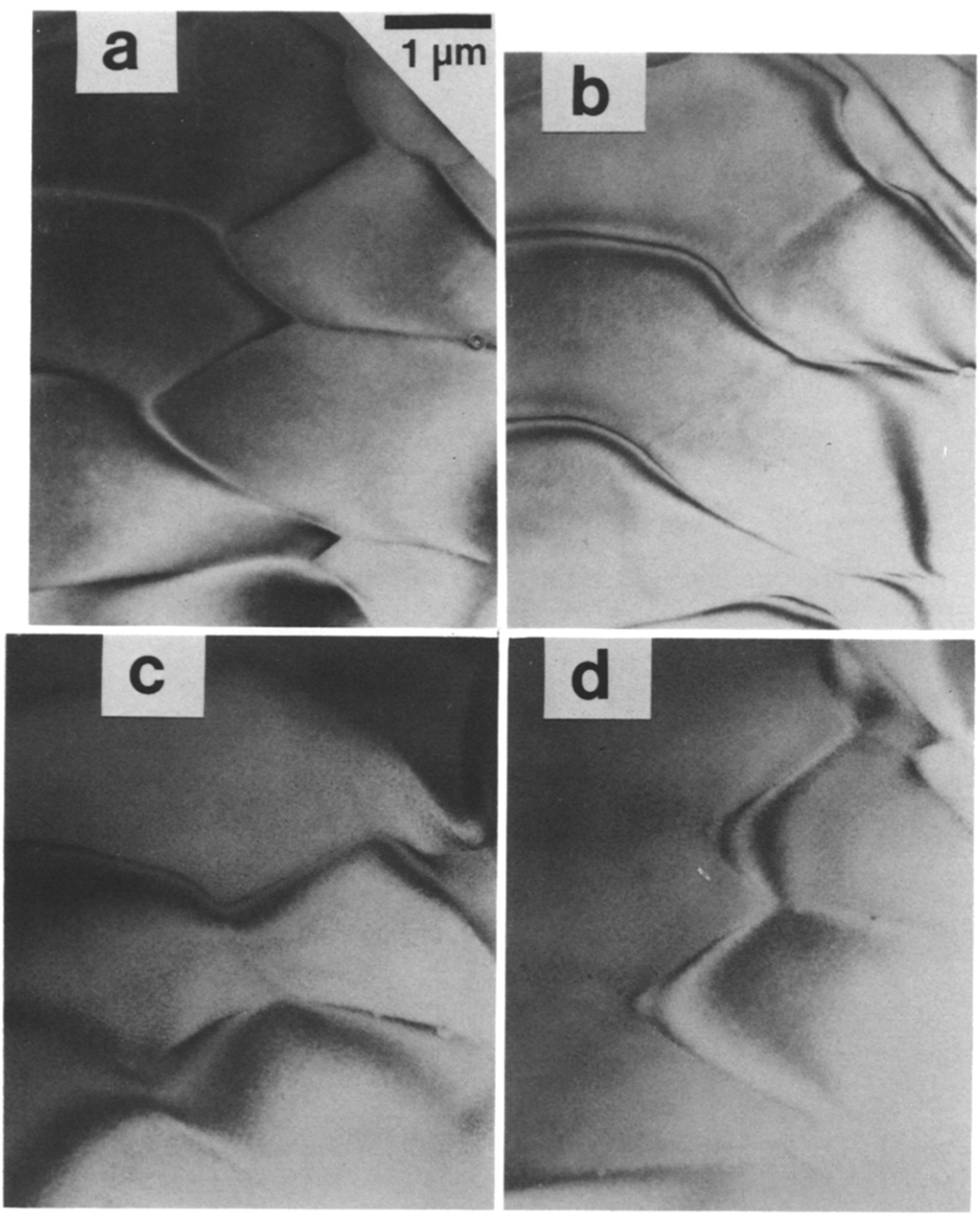

Fig. 7. Contrast experiments on network with irregular geometry in ⟨010⟩ shear-direction sample KP-75. (a) Network under general bright-field imaging conditions. (b) Bright-field, two-beam image for $\mathbf{g} = 020$ showing near invisibility of dislocation segments with $\mathbf{b} = [100]$. (c) Image for $\mathbf{g} = 110$ showing extinction of $\mathbf{b} = 1/2[\bar{1}10]$ segments. (d) Extinction of $\mathbf{b} = 1/2[110]$ segments for $\mathbf{g} = \bar{1}10$.

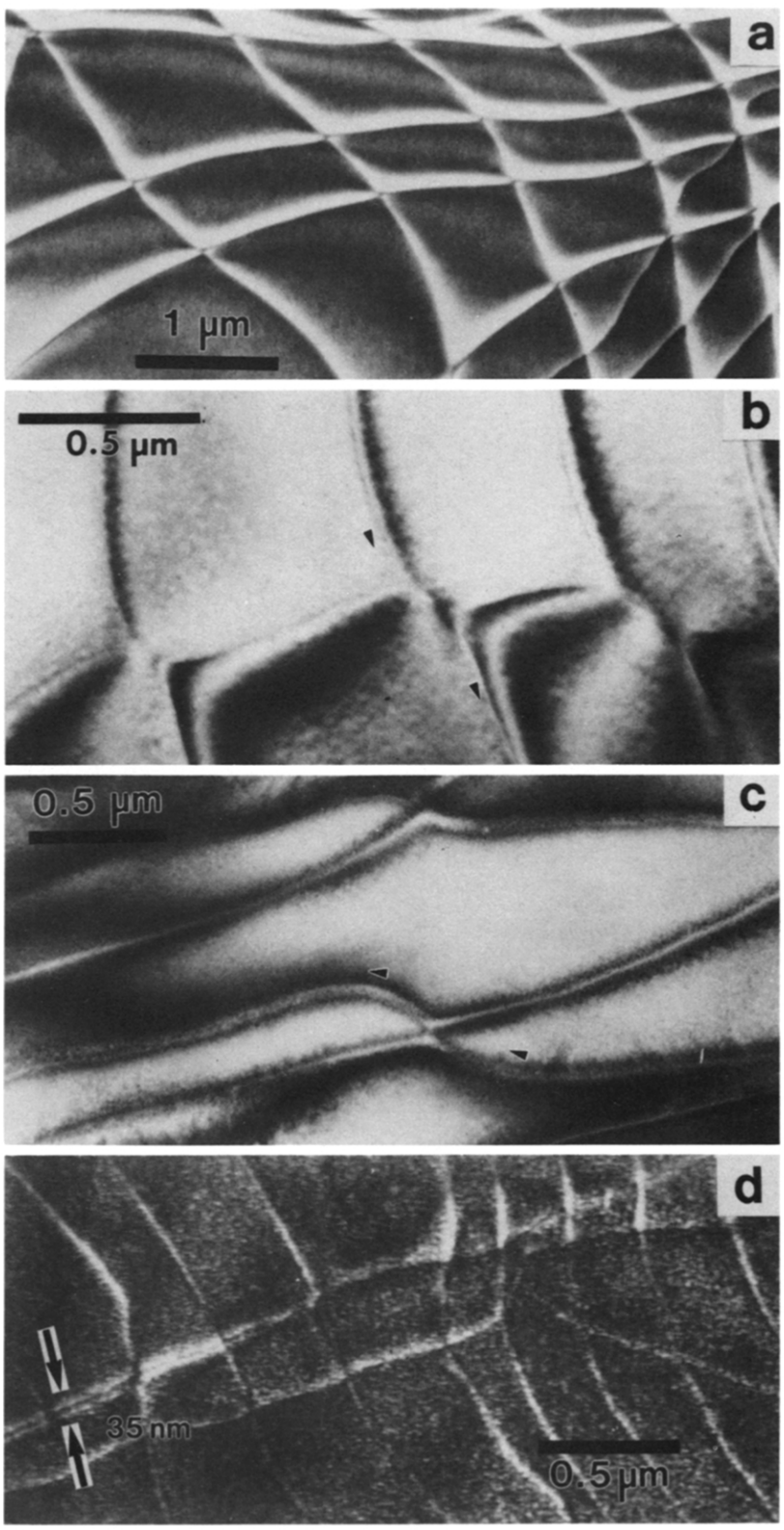

Fig. 8. Images of crossing and superposed dislocations on separate (001) slip planes. (a) Crossing dislocations with no local change in line orientation at crossing points (dark-field image, **g** = 201, sample KP-75). (b) Crossing dislocations that bend to adopt locally parallel or sub-parallel orientations, consistent with mutually attractive interaction (bright-field image, sample KP-75). (c) Crossing dislocations that adopt locally sub-perpendicular line orientations, consistent with mutually repulsive interaction (bright-field image, sample KP-75). (d) Weak-beam image (**g** = 201) of dislocation dipole with projected separation l_x of ~35 nm (sample KP-75).

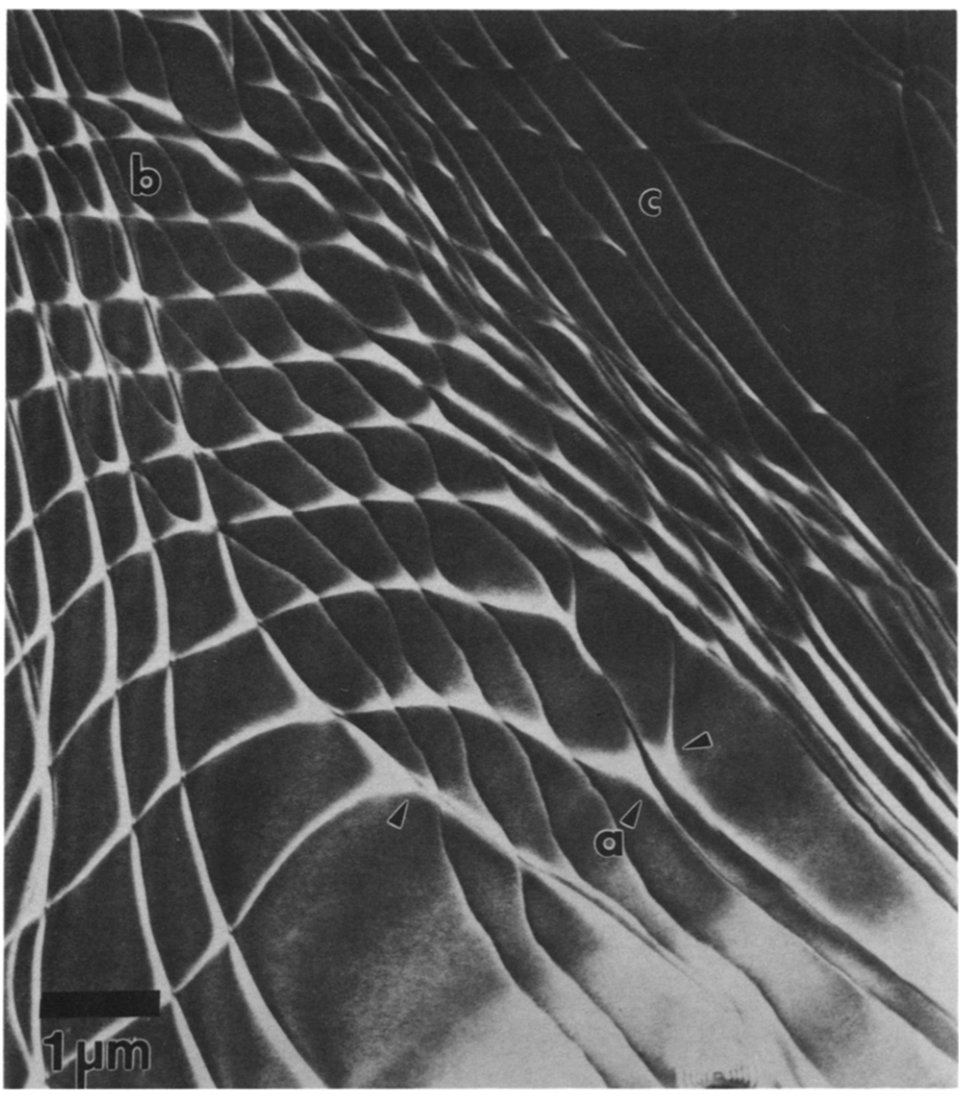

Fig. 9. Dark-field, weak beam, image (**g** = 201) of extended array of dislocations on parallel (001) planes in sample KP-50. Formation of dipoles is evident at points (arrows) where two or more dislocations merge into a single line. Dislocations within more widely-spaced parallel arrays near *a*, generally show more curvature when crossed by other dislocations than dislocations in more closely-spaced parallel arrays near area *b*. Similar behavior is seen in crossing dislocations in area near *c*.

offset may have same-sign Burgers vectors, or may be dipoles on slip planes so closely spaced that the projected separation of the dislocations is less than can be resolved (<10 nm).

In other cases, it was possible to use the characteristic asymmetric contrast of edge dislocations to determine whether merging dislocations were of the same or opposite sign. Based on these criteria, two adjacent edge dislocations whose slip plane separation is less than one extinction distance will show dark or bright contrast on the same side if they are of the same sign, whereas the sense of contrast is reversed for dislocations of opposite sign (Fourie 1964). An example of opposite-sign contrast behavior is shown by dislocations in Fig. 9, which merge to form fairly long, continuous dipole segments. Similar long, curvilinear dipoles have been reported by Steeds & Hazzledine (1964), Amelinckx (1979) and a number of other workers. Finally, we also used the presence or absence of local foil bending across superposed dislocations as evidence that the dislocations were of the same or opposite sign, respectively. Such bending can be recognized by the local displacement of bend contours and changes in background contrast across the dislocations ('kink-contrast') if they are of the same sign (Demny 1963a).

We note that the above criteria work only for dislocations with predominantly edge orientations, and more elaborate contrast experiments are needed to determine the relative sign of superposed screw dislocations. Consequently, we could not unambiguously identify all examples of superposed dislocations as dipoles or stacked dislocations of like sign. Our TEM observations indicate that the superposed and crossing dislocations consist of dipoles as well as pairs of like sign. The dipoles do not contribute to the optical undulatory extinction within samples, whereas paired dislocations of like sign may ultimately give rise to tilt walls, which are evident as optical kink boundaries (Fig. 3a).

Previous analyses of the interaction between two arrays of parallel dislocations that lie on stacked slip planes (Hirth & Lothe 1982, Zhang & Li 1989) provide a basis for estimating the slip plane spacing of crossing dislocations of opposite sign that show attractive interaction. An estimate of this spacing is important as a measure of how closely spaced the glide planes of dislocations need to be before crossing dislocations interact to form dipole segments. Assuming that all the dislocations within each coplanar array have the same sign, but that the two arrays are of opposite sign, a given dislocation is subjected to a repulsive, straightening, force from its coplanar dislocations, its own line tension, and an attractive, bending force from the dislocations in the other plane (Hirth & Lothe 1982, Zhang & Li 1989). The attractive force is derived from the tendency of dislocations of opposite sign in parallel planes to attain equilibrium dipole configurations that are exactly superposed, if the dipole has screw orientation, or offset by a distance l_x viewed normal to the slip plane, if the dipole has edge orientation (Cottrell 1956, Hirth & Lothe 1982).

Zhang & Li (1989) report that the repulsive, straightening, forces on a dislocation in a coplanar array with dislocation spacing l_d will only be overcome by the interplanar attractive forces of another array if the interplanar spacing h of the arrays is less than or equal to $1/4\ l_d$. Consistent with this prediction, within a coplanar array of dislocations of variable spacing, the more widely spaced (large l_d) dislocations should show more curvature due to crossing dislocations on a parallel slip plane than the more closely spaced (small l_d) ones. We have observed this latter phenomenon in our samples (Fig. 9).

For instances where we observed bending of crossing dislocations within superposed arrays with parallel Burgers vectors, we applied Zhang & Li's (1989) criterion in order to estimate upper bounds for h, assuming that these crossing dislocations form dipole segments (Table 2). (However, not all could be unambiguously identified as dipoles). Measurements were based on bent dislocations within arrays of constant spacing l_d as well as in arrays of variable spacing. For arrays of variable spacing we obtained a lower bound for h by noting the value of l_d for which dislocations in the array stopped bending. The absence of significant bending was assessed based on the line length of the crossing dislocations measured according to the geometry outlined in Fig. 10. Using this geometry we compared the increase in line length of dislocations meeting at an angle θ with the maximum increase in line length possible, which is given by:

$$\text{Length}_{max}/\text{Length}_{straight} \cong \sin\theta + \cos\theta, \qquad (1)$$

where Length_{max} is the maximum line length of the interacting dislocations, and $\text{Length}_{straight}$ is the length

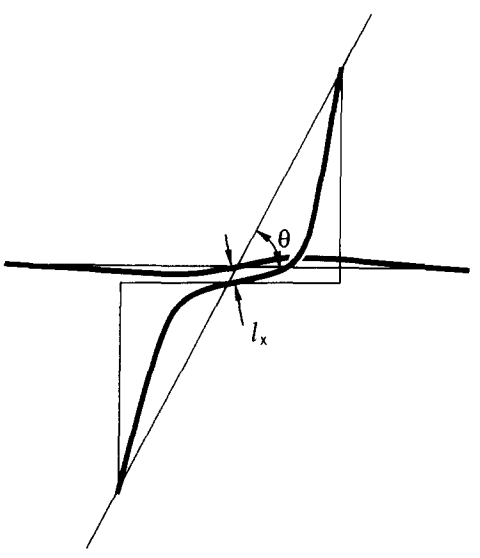

Fig. 10. Geometry of crossing dislocations of opposite sign on parallel (001) planes. Dislocations curve locally to adopt sub-parallel orientations where a finite segment of dipole is formed. A measure of the degree of curvature, and hence of interaction, of the dislocations is obtained by comparing their increase in line length, relative to the maximum increase possible ($\text{Length}_{max}/\text{Length}_{min} \approx \sin\theta + \cos\theta$, with θ measured relative to an adjacent, parallel, unbent dislocation). The distance l_x is the stacking offset of the dislocations, projected on the glide plane (see text).

Table 2. Geometries of crossing dislocations

Sample No.	Shear direction	Mean in-plane spacing of interacting dislocations l_d (μm)	Mean misorientation of crossing dislocations θ (°)	Increase in line length (%)		Stacking offset of dipole l_x† (μm)	Inferred slip plane separation h (μm)		
				Observed	Maximum possible*		Upper/lower bounds‡	Bracketed value§	Edge equilibrium value‖
KP-44	[310]	1.30	85	10	8	—	≤0.32	—	—
KP-50	[110]	1.16	57	24	38	—	≤0.29	—	—
BI-3	[010]	0.27	24	14	32	—	≤0.07	—	—
KP-75	[010]	0.56	21	14	29	—	≤0.14	—	—
KP-75	[010]	0.14	29–54	<2	36–41	—	≥0.035		—
KP-75	[010]	0.23	29–54	<2	36–41	—	≥0.058	0.06–0.12	—
KP-75	[010]	0.46	29–54	5	36–41	—	≤0.12		—
KP-75	[010]	0.65	29–54	6	36–41	—	≤0.16		—
KP-75	[010]	0.21	41	<2	41	—	≥0.052		—
KP-75	[010]	0.54	41	5	41	—	≤0.14	0.05–0.14	—
KP-75	[010]	0.89	41	5	41	0.03–0.04	≤0.22		~0.03–0.04
KP-45	[010]	0.82	7	13	11	—	≤0.21	—	—

*Assuming geometry shown in Fig. 10.
†As determined from weak beam images.
‡Using criterion of Zhang & Li (1989).
§Values of h bracketed by variations noted in geometries of crossing dislocations of variable spacing l_x.
‖Inferred from weak beam images assuming that dipole has reached equilibrium for parallel dislocations, $h \cong l_x$ (Cottrell 1956).

the crossing dislocations would have if they did not interact. Dislocations were considered to show significant curvature only for observed increases in line length of less than 2%. Using these criteria, values of h in sample KP-75 were estimated to be between 0.06 and 0.12 μm for one array, and between 0.05 and 0.14 for another.

A second method to estimate h is based on the maximum value for the stacking offset l_x of the two dislocations that form the dipole segment where the crossing dislocations become locally parallel (Fig. 10). This method assumes that the dislocations within the dipole are forced into their equilibrium spacing by the attractive forces operating along the length of both dislocation lines. As noted above, if the dipole segment has edge orientation, then the dislocations forming the dipole are offset by a distance $l_x = h$, whereas if it has screw orientation, $l_x = 0$ (Cottrell 1956, Hirth & Lothe 1982). Using weak beam images, we determined that l_x was not greater than 0.04 μm, and assuming the dipoles had mostly edge character, we estimate h to be of this order (Table 2).

DISCUSSION

Role of dislocation interactions

The substructure of our experimentally deformed biotite crystals consists of local concentrations of dislocation arrays with a variety of geometries and large regions of crystal that are free of dislocations. Within the arrays there is considerable direct and indirect evidence that dislocations are affected by mutual elastic interactions that may reduce dislocation mobility. Coplanar dislocations with like-sign Burgers vectors repel and ultimately pile-up against one another. Dipoles–multipoles form by the attraction between dislocations of opposite sign on parallel glide planes.

Although interactions may not be as strong between dislocations with non-parallel Burgers vectors, similar in-plane repulsions and attractions between such dislocations on parallel glide planes may occur. Attractive interactions between dislocations with different Burgers vectors on parallel glide planes require closer spacing (smaller h) than for dislocations with parallel Burgers vectors of opposite sign and this is consistent with our observations that crossing dislocations with non-parallel Burgers vectors seldom bend to a locally parallel orientation.

Since dislocations of the same sign on parallel slip planes glide in the same direction, attractive interactions of pairs of such dislocations are not expected to reduce their respective mobility until they become part of a larger tilt wall. Such walls could be formed as part of an overall process of glide polygonization.

For dislocations with different Burgers vectors on the same plane, mobility is strongly determined by the ability of particular dislocations to react and form networks, and by their mobility within these networks. This problem is discussed in a following section. Overall, we consider that most areas of concentrated dislocations represent regions where dislocation motion has been slowed or stopped due to mutual elastic interactions. The dislocation-free areas in turn represent portions of the crystal through which dislocations moved rapidly. This basic set of circumstances is typical of certain stages of dislocation creep in a great many materials, and normally the presence of many glide plane orientations and other factors make it difficult to model the dislocation interactions that control strength. In biotite, however, we believe that the simplified geometry of slip, combined with the information we have obtained on dislocation interactions, permits us to make useful semi-quantitative correlations between flow strength and microstructure. In particular, our observations suggest that dislocation glide in biotite is similar in many respects to that of metals and some oxides deformed by

easy glide. Previous studies of easy glide in metals provide a basis for modeling flow strength–microstructural relations in biotite.

Evidence for easy glide

The stress–strain response of biotite single crystals loaded at 45° to (001) is comparable to that of metals and alloys deformed in orientations that promote glide on a single slip system, and resembles that of hexagonal metals deformed by basal glide as well as FCC single crystals undergoing Stage I easy glide (e.g. Maddin *et al.* 1950, Andrade & Henderson 1951, Seeger *et al.* 1957, Friedel 1964, Hirsch & Lally 1965, Basinski & Basinski 1979). Metals deformed by easy glide are characteristically weak, with strengths $\lesssim 10^{-3}\ G$, where G is the shear modulus. They also show very little strain hardening, with the strain hardening parameter $H = (\partial\sigma/\partial\varepsilon)_{\dot{\varepsilon}}$ generally less than $4 \times 10^{-4}\ G$. The basal shear strengths measured for biotite (Fig. 1 and Table 1) are similarly low when compared with G; using an effective modulus $G = 2.11 \times 10^4$ MPa for shear on (001) (Alexandrov & Ryzhova 1961; Amelinckx 1979), $\tau \cong 9 \times 10^{-4}\ G$ for directions ⟨100⟩ and ⟨110⟩ (at $T = 400$°C and $\dot{\varepsilon} \cong 10^{-5}$ s^{-1}) and $\tau \cong 1.3 \times 10^{-3}\ G$ for directions ⟨310⟩ and ⟨010⟩. Stress–strain curves for biotite do not show strain hardening within experimental uncertainty, consistent with a value of $H < 8$ MPa ($<4 \times 10^{-4}\ G$ or 0.8 MPa over 10% strain).

The low strengths and negligible strain hardening of easy glide have been attributed to the generation and motion of dislocations on a single glide plane, relatively unimpeded by dislocations on other planes or other obstacles. Easy glide may give rise to long slip lines (observed as deflections of polished crystal faces) because of the generation of large numbers of dislocations from individual sources and glide across large fractions of the sample dimensions. Slip lines, typically 100–400 μm, may reach ~1 mm in length (Maddin *et al.* 1950, Seeger *et al.* 1957, 1961, Mader 1963, Hirsch & Lally 1965), and the rate of Stage I hardening H_I has been shown to depend upon crystal size (Suzuki *et al.* 1959). The onset of strong strain-hardening, Stage II deformation in metals is marked by slip on non-parallel planes, dislocation pinning and cross-slip (e.g. Maddin *et al.* 1950, Seeger *et al.* 1957, Mader 1963, Friedel 1964, Hirsch & Lally 1965, Higashida *et al.* 1986). Although slip line studies have not been done on micas, activated slip planes 1–3 μm apart in deformed muscovite have been identified by Bell *et al.* (1986) with large numbers of evenly spaced, slightly bowed dislocations. Moreover, the glide length scales implied by our measurements of KB spacing (Fig. 3 and Table 1) are similar to those reported for easy glide of metals. Slip on non-basal planes of biotite has not been observed and cross-slip of extended screw dislocations across tetrahedral silicate layers of the mica structure is probably difficult. Thus, Stage II deformation of biotite may never be realized.

Many of the dislocation substructures we have observed in deformed biotite samples have been reported in metals deformed by easy glide. Dislocations are distributed inhomogeneously during Stage I deformation of metals, due to the large slip lengths compared with the scale of TEM observations (Seeger *et al.* 1961, Mader 1963, Hirsch & Lally 1965), much as we observe in biotite. Large numbers of dislocations may be generated within the same glide plane and up to 70–80 localized dislocations have been observed in the same plane of deformed Zn and Mg crystals (Seeger *et al.* 1961, Hirsch & Lally 1965). Also similar to our observations for biotite, dislocations in Mg are spaced with distributions that differ markedly from those of large pile-ups (Eshelby *et al.* 1951, Hazzledine & Hirsch 1967). Elastic interactions between dislocations on parallel glide planes are widespread during easy glide of metals with the development of short dipole segments between non-parallel dislocations similar to those recognized in biotite and long, primarily edge dipoles and multipoles (Mader 1963, Steeds & Hazzledine 1964, Hirsch & Lally 1965).

Role of networks

The substructure of deformed biotite crystals differs in a few respects from those of easy-glide metals. Evidence for cross-slip in biotite is lacking, while slip lines in metals appear to terminate where cross-slip has occurred (Maddin *et al.* 1950, Hirsch & Lally 1965). Dislocation walls formed by glide polygonization, as seen in regions of high dislocation density and crack nucleation in mica by Bell *et al.* (1986), are generally only observed in metals once obstacles to the primary slip system during Stage II deformation are significant (Price 1963, Friedel 1964, Hirsch & Lally 1965, Smith 1979). The development of more complicated dislocation arrays in biotite and cracking on cleavage at earlier stages of deformation may be due to heterogeneities in the natural starting material that are less common in the metal crystals and perhaps also due to the inability of dislocations to cross-slip at obstacles.

The presence of well-developed networks in deformed biotite is one of the main microstructural differences between biotite and easy glide metals, which generally do not develop networks until the onset of Stage II hardening (Hirsch & Lally 1965). Whether dislocations can form networks or not, and their ability to continue glide once they have formed networks, may influence their overall mobility. For biotite, coplanar dislocations with different Burgers vectors should interact repulsively, if their Burgers vectors add to the long vectors ⟨010⟩ or 1/2⟨310⟩. Alternatively, they can react to form nodes with a third dislocation if they add to a principal slip vector. Considering the possible node reactions in biotite, it can be shown that for shear along ⟨010⟩ or ⟨310⟩, half of the possible node pair reactions will be of the incompatible, repulsive type, and may reduce dislocation mobilities. The remaining reactions may lead to networks containing a third, sessile, dislo-

cation segment whose Burger vector is normal to the applied shear stress. Within these networks the other dislocations may continue to glide, but their motion is geometrically constrained by the need to react at nodes and simultaneously add and subtract from the lengths of glissile and sessile dislocation segments.

For shear in a principal slip direction ⟨110⟩ or ⟨100⟩, half of the interacting dislocation pairs may experience mutual repulsion. However, the other half form networks in which all of the Burgers vectors are oriented at less than 90° to the principal shear stress. Within these networks dislocation motion is still slowed by the need to lengthen some dislocation segments at the expense of others, but all dislocations of these networks may be mobile. Overall, networks should not prevent the formation of dipole segments and multipoles with dislocations on parallel planes. Thus, the glide mechanisms operating in easy glide materials are expected to be important in biotite, although they may be made somewhat more complicated by additional dislocation interactions.

Relation between microstructure and flow strength

Models of easy glide may be used to explain the mechanical results for biotite and provide a means of understanding the development of obstacles to glide and low-angle kink band boundaries. Dipoles and multipoles much like those observed in our samples play an important role in these models (Hirsch & Lally 1965, Kroupa 1966, Hazzledine 1967) and help explain the lack of significant strain hardening. Deformation at conditions that promote dislocation glide without climb or other mechanisms of recovery generally leads to hardening as the density of dislocations increases and internal stresses accumulate. Internal stresses may be reduced significantly, however, if dislocations become paired as dipoles. The stress fields of dipoles and multipoles decay rapidly with distance as compared with those of isolated dislocations (Li 1963, 1964, Hazzledine 1966) and dislocations in neighboring (001) planes may pass dipoles and multipoles more readily than unpaired dislocations at equivalent distances (Hirsch & Lally 1965, Hazzledine 1966, 1967).

The formation of localized regions of multipoles may occur by nucleation and growth of dislocation loops from sources on parallel (001) planes spaced close enough to permit dislocation interactions (Fig. 11a). If sources operate on planes with spacings small enough relative to the applied stress, dislocations may become trapped and the sources will become inactive. Deformation may proceed elsewhere in the crystal without significant hardening since slip can accelerate on other planes once multipoles are formed. Slip lines have been observed to cluster with increasing strain without much hardening and their spacings are approximately proportional to $1/\varepsilon$ (Hirsch & Lally 1965). The critical shear stress required for one group of dislocations to pass over another group of opposite sign on a parallel plane (Fig. 11b) without forming a multipole (or to decompose an existing multipole) is nearly independent of the number of dislocation pairs n for $n > 6$, and has been given by Hazzledine (1966):

$$\tau_p \cong \frac{Gb}{2\pi kh}, \qquad (2)$$

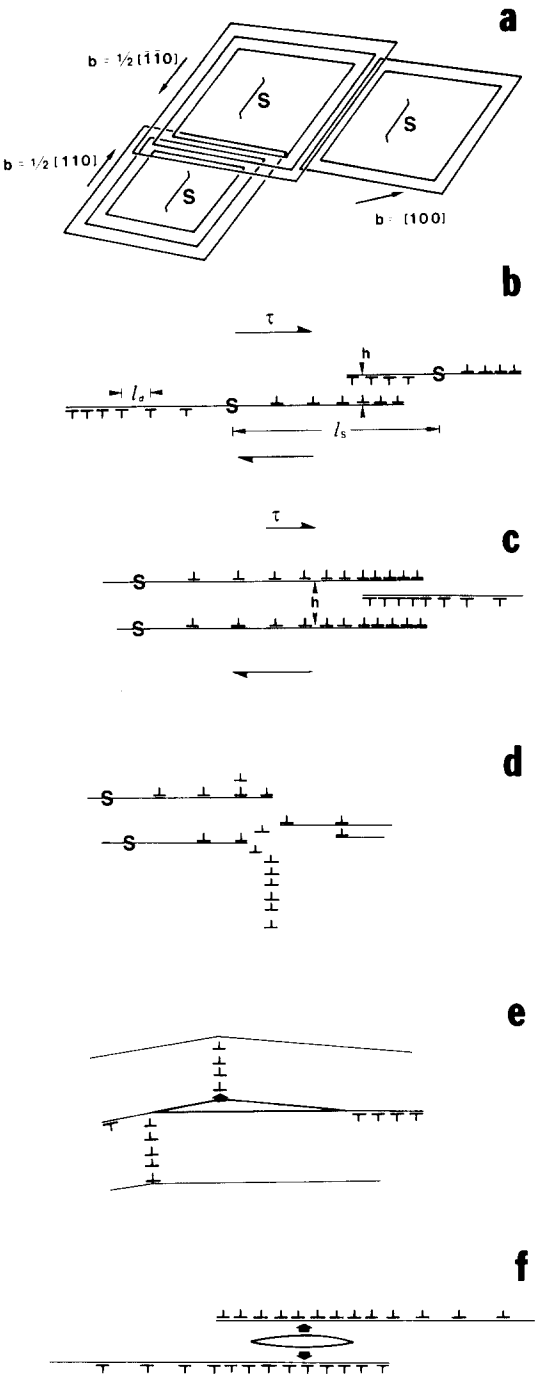

Fig. 11. Dislocation substructures developed during easy glide. (a) Dislocation loops generated at sources S on parallel (001) planes. (Burgers vectors of the loops depend on the local stress state and other factors at the sources.) (b) Stable dipoles and multipoles formed by dislocations of opposite sign generated by sources whose slip plane spacing h is small enough relative to the imposed shear stress τ. Unpaired dislocations with variable spacing l_d occur adjacent to the dipoles. The sources are spaced a distance l_s apart. (c) Pile-up of dislocations of like sign on parallel glide planes. Low-angle KBs form where such pile-ups develop. (d) Excess dislocations of like sign organized into stable dislocation walls by glide polygonization (as observed by Bell *et al.* 1986). (e) Cleavage cracks at high-angle KBs (as seen by Bell *et al.* 1986, Shea & Kronenberg in press) produced by irregular dislocation walls. (f) Cleavage cracks produced by vacancy-type multipoles.

where h is the separation between the slip planes, $k = 4(1 - \nu)$ and $k = 2$ for edge and screw dislocations, respectively, where ν = Poisson's ratio. Dislocations of opposite sign in closely spaced glide planes are easily trapped while those in widely separated planes may pass each other at low stresses. Inferred values of $h \cong 0.03$–$0.06\ \mu$m for dipole segments in sample KP-75 (Table 2) are comparable to values of $h < 0.03\ \mu$m (for edge multipoles) and $h < 0.04$ (for screw multipoles) expected for mutual trapping, assuming that $\tau_p \cong \tau_{001}$ measured (Table 1) and using an effective $\nu = 0.32$ (Alexandrov & Ryzhova 1961, Amelinckx 1979).

Large numbers n of dislocations are observed to localize within dislocation arrays in biotite, much as observed for easy-glide metals. Given n, lower bounds can be placed on the spacing of dislocation sources l_s that form multipoles from relationships between the maximum number of dislocations that can be emitted by each source and the dimensions h and l_s;

$$n \leq \frac{l_s}{6h} \tag{3a}$$

for edge multipoles and

$$n \leq \frac{2l_s}{7h} \tag{3b}$$

for screw multipoles (Hazzledine 1966). Some complications may be expected from the generally mixed character of dislocations in biotite and the occurrence of dislocation reactions and networks in the same plane. However, for $n = 70$–100 dislocations, sources may have spacings l_s on the order of 7–24 μm with mean dislocation spacings l_d of ~0.1.–0.24 μm within the same (001) plane, as compared with the observed dislocation spacing $l_d = 0.54 \pm 0.25\ \mu$m in sample KP-75.

The low-angle kink boundaries observed in thin section must be formed by dislocations of the same sign. We propose that these are formed by the excess dislocations that pile up against multipoles in regions between sources that emit different numbers of dislocations (Fig. 11b). These unpaired dislocations constitute the principal source of internal stress in the easy glide model of Hirsch & Lally (1965). Once dislocation densities are increased, the flow stress τ will depend primarily upon the internal stress τ_i according to the relation:

$$\tau = \tau_o + \tau_{LT} + \tau_i, \tag{4}$$

where τ_o, the frictional stress of glide, and τ_{LT}, associated with increases in line tension, are small. The internal stress applied by a group of dislocations of like sign on a mobile dislocation at a distance r is of the order

$$\tau_i \cong \frac{fGb}{2\pi kr}, \tag{5}$$

where f is the number of excess dislocations of the same sign per pair of sources and k depends on the character of the dislocations as in equation (2) (Hirsch & Lally 1965). If sources generate an average of n dislocations, the excess number of dislocations on one slip plane relative to the other may be estimated as $f \cong \sqrt{2n}$ assuming that excess dislocations of either sign are equally probable for a given pair of sources. Although our TEM observations have not placed any strict constraints on the numbers of dislocations of like sign within individual arrays, values of $f \cong 15$ (or less), given $n \cong 70$–100, are consistent with our TEM observations.

Mean values of f within a sample depend upon the variability with which sources generate dislocations and how many dislocations enter into paired configurations. The high shear strengths observed for samples sheared in directions ⟨310⟩ and ⟨010⟩ relative to those observed for samples sheared in the principal slip directions ⟨100⟩ and ⟨110⟩ may reflect variations in f with direction of shear. For example, repulsive interactions between $\mathbf{b} = [100]$ and $\mathbf{b} = 1/2[110]$ dislocations nucleated at nearby sources in the same (001) plane of samples sheared in the ⟨310⟩ direction may prevent the formation of multipoles with more remote sources. In addition, variations in f (and in h) may occur in samples sheared in ⟨310⟩ and ⟨010⟩ orientations for multipoles formed from opposite sign dislocations with parallel Burgers vectors, and those with non-parallel Burgers vectors (for example [100] and $1/2[\bar{1}\,\bar{1}0]$). Optical observations of low-angle KBs in crystals sheared in directions ⟨010⟩ and ⟨310⟩ suggest that these samples contain greater numbers of dislocations of like sign despite our impression from TEM that dislocation densities, though heterogeneous, are comparable in samples deformed in intermediate and principal slip directions.

The loci of incipient low-angle KBs may develop in regions of the sample in which unpaired dislocations of the same sign accumulate (Fraser *et al.* 1973, Higashida *et al.* 1986). Pile-ups on parallel planes of excess dislocations with the same sign may develop in some regions with increasing strain (Fig. 11c), and act as effective obstacles to glide on other planes (Hazzledine & Hirsch 1967). Internal stresses may alternatively be reduced by glide polygonization (Friedel 1964, Higashida *et al.* 1986) as suggested by the formation of walls (Fig. 11d) nearly perpendicular to (001) as observed by Bell *et al.* (1986). However, unlike subgrain boundaries with evenly spaced dislocations that form with the aid of climb, dislocations in walls formed by glide are likely to be stacked unevenly.

The transition from low-angle KBs in micas that are largely made up of dislocations organized in a variety of configurations to sharply defined, high-angle kink boundaries appears to coincide with the formation of fine-scale cleavage cracks (Bell *et al.* 1986, Shea & Kronenberg in press). Due to the perfect cleavage of micas, this mechanism is likely to be more prevalent than at kink boundaries of other minerals. Nevertheless, cracks parallel to active slip planes in regions of high dislocation density and at kink boundaries have been observed in a variety of other materials (Stokes *et al.* 1962, Price 1963, Friedel 1964, Smith 1979). These cracks nucleate by tensile stresses associated with uneven and complex, offset dislocation walls (Fig. 11e) and vacancy-type multipoles (Fig. 11f) developed during easy glide. Once cleavage cracks open along low-angle

boundaries of biotite, large crystallographic rotations are possible. Contrary to the expectation that kink band boundaries may migrate laterally through the material (Frank & Stroh 1952, Paterson & Weiss 1966, Weiss 1980, Wilson *et al.* 1986, Blumenfeld & Wilson 1991), these high angle boundaries, weakened relative to the surrounding crystal, are likely to be stationary with continued deformation.

The mechanisms that operate during easy glide and the dislocation substructures that develop lead naturally to the mechanical behavior of biotite that we observe, and the nucleation of dilatant high-angle kink boundaries. Easy glide models of biotite deformation are consistent with the conceptual model of Bell *et al.* (1986) and help to characterize the spacing of dislocation sources and identify obstacles to glide.

CONCLUSIONS

Biotite single crystals shortened experimentally in orientations that maximize the critical resolved shear stress on (001) contain dislocations confined to the (001) plane with Burgers vectors 1/2⟨110⟩ and ⟨100⟩, and rare extended dislocations of these same slip systems. Crystals sheared in the direction ⟨110⟩ deform by motion of dislocations with Burgers vectors 1/2[110], as well as 1/2[$\bar{1}$10] and [100] oriented at 60° to the shear direction. Shear in the ⟨310⟩ and ⟨010⟩ directions is accomplished by the combined action of dislocations with complimentary Burgers vectors from the 1/2⟨110⟩ and ⟨100⟩ set that add vectorially to produce slip in the required direction.

The distribution of dislocations is very inhomogeneous in all samples regardless of shear direction, with dislocations concentrated in parallel arrays, networks, and nets of overlapping dislocations on separate (001) planes. Inhomogeneity results from the mutual trapping and localization of dislocations due to repulsive forces between dislocations within the same (001) plane, and attractive forces between dislocations on closely-spaced parallel (001) planes. Dislocation multipoles, formed due to the mutual attraction of opposite-sign dislocations on planes spaced less than ~120 nm apart appear to play a major role in the microstructural evolution of the samples. The pile-up against multipoles of unpaired dislocations with Burgers vectors of the same sign gives rise to internal stresses and may account for the formation and distribution of low-angle kink boundaries.

The dislocation substructures we observe, particularly the formation of multipoles, together with the stress–strain behavior of our samples, all indicate that biotite deforms by easy-glide. Easy glide models provide a framework for understanding how obstacles to glide originate in biotite, and how these obstacles control strength. These models can be extended to account for microstructural features such as dilatant high-angle kink boundaries that are characteristic of micas.

Acknowledgements—This study was supported by National Science Foundation collaborative research grants EAR-8816283 to A. K. Kronenberg and EAR-8816622 to R. Christoffersen. Transmission electron microscopy was carried out in the Electron Microscopy Center at Texas A&M University and the Central Facility for Electron Microscopy at the University of Pennsylvania, which is supported by the National Foundation, MRL program, under grant No. DMR 88-19885. Technical support at the Penn Central TEM facility was provided by D. Ricketts-Foote. We thank R. McNeely and M. Beal for cheerfully typing the tables and several versions of this paper. The paper benefited greatly from review comments made by Steve Kirby and an anonymous reviewer. Finally, thanks go to John Christie for sharing his humor, for surprising the local southern Cal undergraduates with his unique field wardrobe, and for convincing A. K. Kronenberg to forget about measuring deformed ooids in -€ p-7 of the Poletta Formation.

REFERENCES

Alexandrov, K. S. & Ryzhova, T. V. 1961. Elastic properties of rock-forming minerals. II. Layered silicates. *Bull. (Izv.) Acad. Sci. USSR, Geophys. Ser.* **12**, 1165–1168.

Amelinckx, S. 1979. Dislocations in particular structures. In: *Dislocations in Solids, Volume* 2 (edited by Nabarro, F. R. N.). North-Holland, Amsterdam, 67–460.

Amelinckx, S. & Delavignette, P. 1962. Dislocations in layer structures. In: *Direct Observations of Imperfections in Crystals* (edited by Newkirk, J. B. & Wernick, J. H.). Wiley-Interscience, New York, 295–356.

Amelinckx, S. & Delavignette, P. 1963. Dislocations in layer structures. In: *Electron Microscopy and Strength of Crystals* (edited by Thomas, G. & Washburn, J.). Wiley-Interscience, New York, 441–513.

Amelinckx, S. & Van Landuyt, J. 1976. Contrast effects at planar interfaces. In: *Electron Microscopy in Mineralogy* (edited by Wenk, H.-R.). Springer, Berlin, 68–73.

Andrade, E. N. da C. & Henderson, C. 1951. The mechanical behaviour of single crystals of certain face-centered cubic metals. *Phil. Trans. R. Soc. Lond.* **A244**, 177–203.

Baños, J. O. 1985. Interlayer energy for partial slip and cleavage in muscovite. *Phil. Mag.* **A52**, 145–152.

Baños, J. O., Amouric, M., DeFouquet, C. & Baronnet, A. 1983. Interlayering and interlayer slip in biotite as seen by HRTEM. *Am. Miner.* **68**, 754–758.

Baronnet, A. & Olives, J. 1983. The geometry of micas around kink band boundaries, I. A crystallographic model. *Tectonophysics* **91**, 359–373.

Basinski, S. J. & Basinski, Z. S. 1979. Plastic deformation and work hardening. In: *Dislocations in Solids, Volume* 4 (edited by Nabarro, F. R. N.). North-Holland, Amsterdam, 261–362.

Behrmann, J. H. 1984. A study of white mica microstructure and microchemistry in a low grade mylonite. *J. Struct. Geol.* **6**, 283–292.

Bell, I. A. & Wilson, C. J. L. 1977. Growth defects in metamorphic biotite. *Phys. Chem. Miner.* **2**, 153–169.

Bell, I. A. & Wilson, C. J. L. 1981. Deformation of biotite and muscovite: TEM microstructure and deformation model. *Tectonophysics* **78**, 201–228.

Bell, I. A., Wilson, C. J. L., McLaren, A. C. & Etheridge, M. A. 1986. Kinks in mica: role of dislocations and (001) cleavage. *Tectonophysics* **127**, 49–65.

Blumenfeld, P. R. & Wilson, C. J. L. 1991. Boundary migration and kinking in sheared napthalene. *J. Struct. Geol.* **13**, 471–483.

Borg, I. & Handin, J. 1966. Experimental deformation of crystalline rocks. *Tectonophysics* **3**, 249–368.

Carter, N. L. & Tsenn, M. C. 1987. Flow properties of continental lithosphere. *Tectonophysics* **136**, 27–63.

Cottrell, A. H. 1956. *Dislocations and Plastic Flow in Crystals.* Clarendon Press, Oxford.

Demny, J. 1963a. Elektronenmikroskopische Untersuchungen an sehr dünnen Glimmer folien, I. *Z. Naturforsch.* **A18a**, 1088–1096.

Demny, J. 1963b. Elektronenmikroskopische Untersuchungen an sehr dünnen Glimmer folien, I. *Z. Naturforsch.* **A18a**, 1097–1101.

Eshelby, J. D., Frank, F. C. & Nabarro, F. R. N. 1951. The equilibrium of linear arrays of dislocations. *Phil. Mag.* **42**, 351–364.

Etheridge, M. A., Hobbs, B. E. & Paterson, M. S. 1973. Experimental deformation of single crystals of biotite. *Contr. Miner. Petrol.* **38**, 21–36.

Evans, B. & Dresen, G. 1991. Deformation of earth materials: six easy pieces. *Rev. Geophys.* **29**, 823–843.

Fourie, J. T. 1964. Dislocation dipoles in deformed copper single crystals. *Phil. Mag.* **10**, 1027–1041.

Frank, F. C. & Stroh, A. N. 1952. On the theory of kinking. *Phys. Soc. Proc. Ser.* **B65**, 811–821.

Fraser, H. L., Loretto, M. H. & Smallman, R. E. 1973. The plastic deformation of NiAl single crystals between 300K and 1050K. II. the mechanism of kinking and uniform deformation. *Phil. Mag.* **28**, 667–677.

Friedel, J. 1964. *Dislocations*. Pergamon Press, Oxford.

Hazzledine, P. M. 1966. Dislocation multipoles. *J. Phys. Colloq. C3* **27**, C3-210–C3-218.

Hazzledine, P. M. 1967. Work hardening in easy glide. *Can. J. Phys.* **45**, 765–775.

Hazzledine, P. M. & Hirsch, P. B. 1967. A critical examination of the long-range stress theory of work-hardening. *Phil. Mag.* **15**, 121–159.

Higashida, K., Takamura, J. & Narita, N. 1986. The formation of deformation bands in f.c.c. crystals. *Mater. Sci. Engng* **81**, 239–258.

Hirsch, P. B. & Lally, J. S. 1965. The deformation of magnesium single crystals. *Phil. Mag.* **12**, 595–648.

Hirth, J. P. & Lothe, J. 1982. *Theory of Dislocations*. Wiley–Interscience, New York.

Kanaori, Y., Kawakami, S. & Yairi, K. 1991. Microstructure of deformed biotite defining foliation in cataclasite zones in granite, Central Japan. *J. Struct. Geol.* **13**, 777–785.

Kirby, S. H. 1985. Rock mechanics observations pertinent to the rheology of the continental lithosphere and the localization of strain along shear zones. *Tectonophysics* **119**, 1–27.

Kronenberg, A. K., Kirby, S. H. & Pinkston, J. 1990. Basal slip and mechanical anisotropy of biotite. *J. geophys. Res.* **95**, 19,257–19,278.

Kroupa, F. 1966. Dislocation dipoles and dislocation loops. *J. Phys. Colloq. C3* **27**, C3-154–C3-167.

Li, J. C. M. 1963. Theory of strengthening by dislocation groupings. In: *Electron Microscopy and Strength of Crystals* (edited by Thomas, G. & Washburn, J.). Interscience, New York, 713–778.

Li, J. C. M. 1964. Interaction of dislocation dipoles. *Discuss. Faraday Soc.* **38**, 138–146.

Lister, G. S. & Snoke, A. W. 1984. S–C mylonites. *J. Struct. Geol.* **6**, 617–638.

Maddin, R., Mathewson, C. H. & Hibbard, W. R. 1950. The active slip systems in the simple axial extension of single crystalline alpha brass. *Trans. Am. Inst. Min. Metall. Engrs* **185**, 527–534.

Mader, S. 1963. Surface and thin-foil observations of the substructure in deformed FCC and HCP metal single crystals. In: *Electron Microscopy and Strength of Crystals* (edited by Thomas, G. & Washburn, J.). Interscience, New York, 183–228.

Mares, V. M. & Kronenberg, A. K. 1993. Experimental deformation of muscovite. *J. Struct. Geol.* **15**, 1061–1075.

Meike, A. 1989. In situ deformation of micas: a high voltage electron microscope study. *Am. Mineral.* **74**, 780–796.

Paterson, M. S. & Weiss, L. E. 1966. Experimental deformation and folding in phyllite. *Bull. geol. Soc. Am.* **77**, 343–374.

Price, P. B. 1963. Direct observations of glide, climb, and twinning in hexagonal metal crystals. In: *Electron Microscopy and Strength of Crystals* (edited by Thomas, G. & Washburn, J.). Interscience, New York, 41–129.

Seeger, A., Diehl, J., Mader, S. & Rebstock, H. 1957. Work-hardening and work-softening of face-centered cubic metal crystals. *Phil. Mag.* **2**, 323–350.

Seeger, A., Kronmüller, H., Mader, S. & Träuble, H. 1961. Work-hardening of hexagonal close-packed crystals and in the easy glide region of face-centred cubic crystals. *Phil. Mag.* **6**, 639–655.

Shea, W. T. & Kronenberg, A. K. In press. Rheology and deformation mechanisms of an isotropic mica schist. *J. geophys. Res.*

Silk, E. C. H. & Barnes, R. S. 1961. The observation of dislocations in mica. *Acta Metall.* **9**, 558–562.

Smith, E. 1979. Dislocations and cracks. In: *Dislocations in Solids, Volume* 4 (edited by Nabarro, F. R. N.). North-Holland, Amsterdam, 363–448.

Starkey, J. 1968. The geometry of kink bands in crystals—a simple model. *Contr. Miner. Petrol.* **19**, 133–141.

Steeds, J. W. & Hazzledine, P. M. 1964. Dislocation configurations in deformed copper and copper 10% (atomic) aluminium alloy. *Discuss. Faraday Soc.* **38**, 103–110.

Stokes, R. J., Johnston, T. L. & Li, C. H. 1962. Kinking and the fracture of ionic solids. *J. appl. Phys.* **33**, 62–67.

Suzuki, H., Ikeda, S. & Takeuchi, S. 1959. Deformation of thin copper crystals. *J. Phys. Soc. Jap.* **11**, 382–393.

Weiss, L. E. 1980. Nucleation and growth of kink bands. *Tectonophysics* **65**, 1–38.

Wilson, C. J. L. 1980. Shear zones in a pegmatite: a study of albite–mica–quartz deformation. *J. Struct. Geol.* **2**, 203–209.

Wilson, C. J. L. & Bell, I. A. 1979. Deformation of biotite and muscovite: optical microstructure. *Tectonophysics* **58**, 179–200.

Wilson, C. J. L., Burg, J. P. & Mitchell, J. C. 1986. The origin of kinks in polycrystalline ice. *Tectonophysics* **127**, 27–48.

Zhang, L. & Li, Z. 1989. Some special types of low energy dislocation configurations in annealed α-Ti single crystals. *Mater. Sci. Engng* **A113**, 185–190.